# Joint Estimation of Telescope Drift and Space Object Tracking

Oksana Hagen, Jérémie Houssineau, Isabel Schlangen, Emmanuel D. Delande, Jose Franco and Daniel E. Clark
School of Engineering and Physical Sciences
Heriot-Watt University
Edinburgh EH14 4AS, UK
{oh35, j.houssineau; is117; e.d.delande, jf139; d.e.clark}@hw.ac.uk

*Abstract*—**With the proliferation of low-cost CCD-based sensors used on telescopes by amateur astronomers, there is potential to exploit these within an infrastructure for space surveillance. Observations may be corrupted by an undesirable drift of the telescope due to mount jittering and uncompensated diurnal motion of stars. This work presents an approach for drift compensation based on a joint estimation of the sensor drift and the states of the objects and stars observed by the telescope. It exploits a recent development in multi-object estimation, known as the single-cluster Probability Hypothesis Density filter, that was designed for group tracking. The sensor drift is obtained by estimating the collective motion of the stars, which is in turn used to correct the estimation of moving objects. The proposed method is illustrated on simulated and real data.**

## Table of Contents

## 1. Introduction

Objects with close proximity to Earth are of special interest in the context of Space Situational Awareness (SSA) [1]. They include Earth-orbiting objects and near-Earth objects, as well as small solar system bodies, typically comets or asteroids whose orbit intersects the orbit of the Earth. While the latter are generally of a few kilometres size and are currently monitored because of their potential collision with Earth, the first category comprises relatively small objects which endanger currently active satellites, ongoing and future space missions.

The data to evaluate such risks are obtained by complex networks of sensors like radars, radio and optical telescopes [2], [3]. Measurements are integrated to build a reliable prediction of future events to avoid unwanted collisions in the sky. However, because of the imperfections in the mechanical systems used for telescope pointing, the recorded data may be corrupted by jitter [4]. Other possible sources of disturbance in astronomical images include atmospheric perturbation as well as basic camera jitter [5].

There are two possible modes for operating telescopes. Either the telescope corrects the diurnal motion of the celestial bodies or it is positioned with a constant pointing direction in horizontal coordinates. In both cases, basic random drift will appear due to the jitter of the mount, and in the latter case, an additional approximately linear component will be observed in case of short acquisition times.

Since the precise pointing direction of the telescope is crucial for defining the astrometric coordinates of the target, it is of great importance to keep its error as small as possible. Even slight perturbations in altitude and azimuth result in large astrometric shift. Various control techniques are used for directing the mount and correcting for possible uncertainties. Optional built-in correction software can help to compensate for certain types of perturbation provided that they are repeatable and static on the hardware side [6], [7], [8].

Since computational power has become more accessible in the last decades, some of the methods now use digital image registration, e.g. [9]. Conventional image registration methods, however, rely heavily on the extraction of fiducial feature points [10]. Other output-correction approaches are defined solely on guide star catalogues (such as the Tycho Catalog or Guide Star Catalogue 2) in an attempt to match the pattern of the stars [11], [12].

Typically, the problem of image misalignment is solved separately from object tracking. However, it is possible to integrate the estimation of the sensor drift and the multiple object states within a single probabilistic framework, so that the improved sensor drift estimate yields to an improved multi-object state estimate, and vice versa. In the scope of this article, the joint estimation problem consists in a simultaneous estimation of the telescope drift and the motion of the observed objects such as space debris, satellites, or stars. The presented technique is based on a hierarchical model in which the measurements are conditioned on the object states and the location of the sensor [13], [14], [15], [16], [17]. A multi-object filter estimates simultaneously the stars in the background and the objects moving in the sensor Field of View (FoV), while the motion of the sensor is observed indirectly by estimating the collective motion of the stars.

The methodology of this article is explained in Sec. 2-6. An explanation of the joint drift compensation and multi-object estimation problem is given in Section 2, and the two aspects of multi-object state and sensor state estimation are treated separately in Sec. 3 and 4. Since the acquisition of the measurements from the astronomic images is an important aspect of the estimation, the preprocessing flow and observation extraction are presented in Sec. 5, demonstrated on the data that is used for the experiments. After that, the process of dataset simulation for the experimental section is explained

in Sec. 6. The results in Sec. 7 are divided according to the data used (simulated and real) as well as the model of drift. The registered multi-object tracking results obtained from the simulated data are given along with error plots with respect to (w.r.t.) the simulated ground truth; for the real datasets, only qualitative estimation is presented since no ground truth is available in this case. The set of parameters that was used for the tests is also specified in this section. The paper concludes in Sec. 8.

## 2. JOINT ESTIMATION PROBLEM

During a surveillance scenario, the sensor focusses on a region of space delimited by its FoV and produces a sequence of image frames from successive observations across time. For the rest of the paper, the time is indexed on the sequence of images corresponding to a specific surveillance scenario.

It cannot always be guaranteed that the acquired images are perfectly registered because of small jitter of the telescope or large-scale bias due to the diurnal motion of Earth. In other words, the observation process is corrupted by *sensor drift*. In this paper, the drift at time $t$ is modeled with a *sensor state* $y_t$, a 4-dimensional vector in some *sensor state space* $\mathcal{Y} \subseteq \mathbb{R}^4$ describing the deviation of the sensor in the image plane w.r.t. to the initial frame, with two position followed by two velocity components.

Following the technique presented in Sec. 5, a set of *measurements* (or *observations*) is extracted from each image frame. Each measurement is characterized by its *state* $z_t$, a 2-dimensional vector in some *observation space* $\mathcal{Z} \subseteq \mathbb{R}^2$ describing the position coordinates of the measurement in the image plane. We denote the set of measurements collected at time $t$ by $Z_t$.

Finally, each object in the sensor FoV at time $t$ is characterized by its *state* $x_t$, a 4-dimensional vector in some *target state space* $\mathcal{X} \subseteq \mathbb{R}^4$ describing the position and then velocity coordinates of the object in the image plane. The set $X_t$ denotes the current *multi-object state*, i.e., the set of all the states of the objects present in the sensor FoV.

The main challenge in this estimation problem is that the sensor drift corrupting the observation data is *unknown*, and thus must be estimated alongside the object states. Fortunately, the static nature of the stars in the image background can be exploited for calibration purposes since the drift of the sensor manifests itself in the synchronised movement of all static objects in the scene.

In this paper, we introduce a probabilistic method exploiting a Simultaneous Localisation and Mapping (SLAM) based approach [14], in which the sensor drift is estimated *jointly* with the states of the objects observed in the sequence of images. The algorithm follows a hierarchical structure, depicted in Fig. 1 (both target and sensor state spaces are reduced to two dimensions for the sake of illustration). The joint estimator is structured as a single-cluster Probability Hypothesis Density (PHD) filter as follows:

1. The sensor state estimator is implemented with a Sequential Monte Carlo (SMC) method, i.e., a *particle filter*;

2. Each particle, corresponding to an admissible value of the sensor state, is associated to a PHD filter [18] estimating the multi-object state.
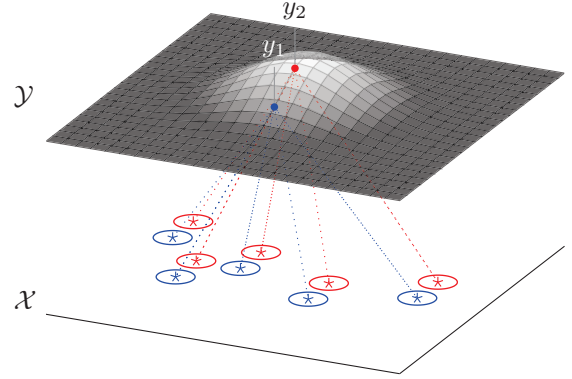


**Figure 1**: **The hierarchical structure of the algorithm (illustrated in 2D). The sensor state space $\mathcal{Y}$ is overlayed by the probability distribution of the sensor position. A specific multi-object distribution in the target state space $\mathcal{X}$ is maintained for each possible sensor position (blue and red colours for sensor positions $y_1$ and $y_2$, respectively). The asterisks and ellipses illustrate the means and covariances of the targets, extracted from the multi-object distributions.**

The PHD filter [18] is selected for the design of the multi-object estimator because it focusses on the estimation of *populations* of objects and avoids the frame-to-frame association of individual objects. In addition, the sensor state estimator is expected to inherit the robustness of the underlying PHD filtering framework to imperfections in the data – most notably, missed detections and clutter observations – through the hierarchical structure of the joint estimator.

An important characteristic of the proposed method is that the PHD filtering framework incorporates a probabilistic classification of the objects following a range of $M$ different motion models[2], for the static objects in the sensor frame – typically, the stars in the background – play an important role in the estimation of the sensor state.

## 3. MULTI-OBJECT ESTIMATION

The exploitation of the PHD filter for the estimation of the multi-object state is central to the performance of the proposed sensor calibration method presented in Sec. 4. An alternative method has been exploited in [17] where the Hypothesised filter for Independent Stochastic Populations (HISP) [19] has been used for calibrating video sequences in microscopy, using one object motion model only. Other works like [14], [15] or [16] utilise the PHD filter with a single motion model for the objects.

The PHD filter is set within the Random Finite Set (RFS) filtering framework, in which the information about the multi-object state $X_t$ is represented by a single random variable called a multi-object RFS $\Phi$. A realisation of $\Phi$ is a set $X = \{x_1, \dots, x_n\}$ of points belonging to the single object state space $\mathcal{X}$. The multi-object RFS $\Phi$ can be seen as a set whose size and elements are random, able to represent the uncertainties in the number *and* the states of the objects in

---

[2]In the experiments presented in Sec 7 only two motion models – *static* and *moving* objects – are considered. In the general case, however, any number of motion models could be assumed.

the sensor FoV [18]. In its usual form, the PHD filter aims at propagating the first-order moment density or *intensity* $\mu_t$ of the multi-object RFS $\Phi$, defined on the state space $\mathcal{X}$; it is such that the expected number of objects in some arbitrary region $F \subseteq \mathcal{X}$ of the target state space is given by the integral $\int_F \mu_t(x)\mathrm{d}x$.

For the rest of this section, $y \in \mathcal{Y}$ denotes an aritrary sensor state, upon which the observation process is conditioned. The PHD filtering framework [18] is based on the following modelling assumptions (at time $t$):

- An object with state $x_{t-1}$ in time step $t-1$ survives to the current time step with probability $p_{\mathrm{s},t}(x_{t-1})$, where $p_{\mathrm{s},t}$ is the probability of survival. If it survives, it evolves to a new state $x_t$ according to a single-object Markov transition density $f_t(\cdot|x_{t-1})$;
- Newborn objects appear in the scene, independently of the pre-existing targets, following a birth process with given intensity $\gamma_t$;
- An object with current state $x_t$ is detected by the sensor with probability $p_{\mathrm{d},t}(x_t|y)$. If it is detected, it produces an observation $z$ according to a single-observation/single-object likelihood $g_t(z|x_t, y)$;
- False alarms are produced in the observation space independently of the targets, following a clutter process with intensity $\lambda_t(y)c_t(z|y)$.

A detailed construction of the resulting PHD filtering equations can be found in [18].

In contrast to the usual PHD filter, which represents the *whole* population of objects with a single RFS, the method presented in this paper aims at estimating *different* population of objects for each considered motion model.

Assuming that the number of motion models is set to $M = 2$, and denoting by $\Phi^{(m)}$ the RFS representing the population of objects following the motion model $m$, one iteration of the PHD recursion with multiple motion models can be visualised in the following diagram:
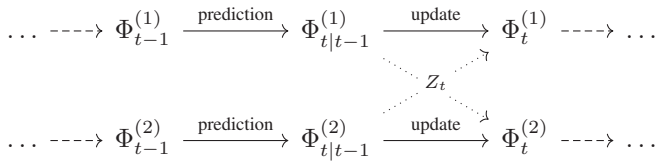


In the prediction step, each population is propagated independently according to its own probability of survival $p_{\mathrm{s},t}^{(m)}$ and Markov transition density $f_t^{(m)}$, and the birth process generates targets for both populations. However, the update step has to be performed in a joint manner since the observed measurement set $Z_t$ carries information for both populations. This is ensured by treating the objects of the first population, in the update step of the second population, as "undesirable" sources of observation that are not to be estimated, and vice versa.

The resulting PHD filtering equations are given as follows. Given an aritrary motion model $1 \leq m \leq M$, the prediction equation of the $m$th population is

$$\mu_{t|t-1}^{(m)}(x|y) = \int p_{\mathrm{s},t}^{(m)}(\bar{x})f_t^{(m)}(x|\bar{x})\mu_t^{(m)}(\bar{x}|y)\mathrm{d}\bar{x} + w_t^{(m)}\gamma_t(x),$$
(1)

where the model weights $w_t^{(m)}$, distributing the birth component among the motion models, are such that $\sum_{m=1}^{M} w_{\mathrm{b},t}^{(m)} = 1$. The update equation of the $m$th population is then

$$\mu_t^{(m)}(x|y) = (1 - p_{\mathrm{d},t}(x|y))\mu_{t|t-1}^{(m)}(x|y)$$

$$+ \sum_{z \in Z_t} \frac{p_{\mathrm{d},t}(x|y)g_t(z|x,y)\mu_{t|t-1}^{(m)}(x|y)}{\lambda_t(y)c_t(z|y) + \sum_{\bar{m}=1}^{M} \int p_{\mathrm{d},t}(\bar{x}|y)g_t(z|\bar{x},y)\mu_{t|t-1}^{(\bar{m})}(\bar{x}|y)\mathrm{d}\bar{x}}.$$

Note that the joint normalisation in the update equation (2) accounts for the interaction between the different motion models.

## 4. SENSOR STATE ESTIMATION

The estimation of the sensor state is maintained by a set of $N$ weighted particles $\{(w_t, y_t)^i\}_{i=1}^N$, where $y_t^i \in \mathcal{Y}, 1 \leq i \leq N$, is a possible sensor state with associated weight $w_t^i$.

For every considered motion model $1 \leq m \leq M$ and every sensor state $1 \leq y_t^i \leq N$, a specific PHD filter propagates the intensity $\mu_t^{i,(m)}(\cdot) = \mu_t^{(m)}(\cdot|y_t^i)$, estimating the population of objects following the $m$th motion model conditioned on sensor state $y_t^i$ (see Sec. 3 for more details).

Like every Bayesian approach, the estimation of the sensor state can be described in three steps: *initialisation*, *time prediction*, and *data update*, the last two ones being repeated sequentially across time whenever a new measurement set $Z_t$ becomes available.

1. *Initialisation* (time 0): Without loss of generality, the initial sensor drift is set at zero. All particle states $y_0^i$ are thus initialized with the null vector, and with uniform weights $w_0^i = 1/N$. The sensor FoV is assumed void of any target at the initial step, and thus all the intensities $\mu_0^{i,(m)}$ are set to zero as well.

2. *Prediction* (time $t$): Each particle is sampled according to a drift motion model $h_{t|t-1}$, depicting the knowledge of the operator regarding the evolution of the sensor drift since the last time step[3], i.e.

$$y_t^i \sim h_{t|t-1}(\cdot|y_{t-1}^i).$$
(2)

In addition, the intensities $\mu_t^{i,(m)}$ are predicted independently using the corresponding object motion model $m$ as shown in Eq. (1).

3. *Update* (time $t$): The weight of the $i$th particle is updated based on the underlying PHD filter update conditioned on the new measurement set $Z_t$ in order to evaluate the match of the proposed sensor state $y_t^i$ with the newly available measurements. The dependence of the likelihood function $g_t$ on the sensor state $y_t^i$ in Eq. (2) is incorporated straightforwardly by subtracting the bias induced by the drift $y_t^i$ from all the measurements $z \in Z_t$. There are typically many static targets in the sensor FoV – most notably, the stars in the background – and they are reliable features for sensor

---

[3]Several drift motion models are considered in the experiments, see Sec. 7 for more details.

calibration. Therefore, only the static objects are used for estimation of the sensor drift in the context of this paper. For the rest of the paper, the index $m = 1$ will denote the motion model corresponding to static objects. The re-weighting of the $i$th particle is computed through the likelihood given by

$$\mathcal{L}(Z_t|\mu_t^{i,(1)}, y_t^i) = \frac{\hat{\mathcal{L}}(Z_t|\mu_t^{i,(1)}, y_t^i)}{\sum_{i=1}^{N} \hat{\mathcal{L}}(Z_t|\mu_t^{i,(1)}, y_t^i)} \quad (3)$$

with

$$\hat{\mathcal{L}}(Z_t|\mu_t^{i,(1)}, y_t^i) = \exp\left(-\int p_{\mathrm{d},t}(x|y_t^i)\mu_t^{i,(1)}(x)\mathrm{d}x\right) \times$$
$$\prod_{z \in Z_t} \left(\lambda_t(y_t^i)c_t(z|y_t^i) + \int p_{\mathrm{d},t}(x|y_t^i)g_t(z|x, y_t^i)\mu_t^{i,(1)}(x)\mathrm{d}x\right). \quad (4)$$

A roulette resampling [20] is then performed whenever the effective sample size

$$N_{\mathrm{eff}} = \frac{1}{\sum_{i=1}^{N}(w_t^i)^2} \quad (5)$$

is such that the ratio $\frac{N_{\mathrm{eff}}}{N}$ falls below some threshold value $\tau$.

# 5. EXTRACTION

This section explains the method that was used to extract position measurements from objects in a sequence of astronomical images.

The real data for the experiments was obtained using a cooled *Starlight Xpress SXV-M7* CCD camera with 250mm f4.3 Newtonian reflector. As an example, one frame from the first dataset is shown in Fig. 2a.

The target trail is quite faint in both image sequences while the intensity of the stars is very high (see Fig. 2c). The image is thus rescaled to increase the contrast, using a logarithmic scale. The resulting image is shown in Fig. 2b along with its histogram in Fig. 2d.

The subsequent step eliminates differences in the illumination caused by irregularities of the sensor using background subtraction

$$\bar{I} = I - I \circ D \quad (6)$$

where $I$ denotes the original image, $\bar{I}$ is the resulting image and $D$ is a structuring element in a shape of a disk with radius $r > 3$, and the operation $\circ$ denotes morphological opening (see Fig. 2e). After that, the image is convolved with a Gaussian smoothing kernel with a standard deviation of 0.5 pixels in order to remove high frequency noise (see Fig. 2f).

To create a binary mask for further connected component analysis, the smoothed image is binarised by thresholding using an empirical threshold value corresponding to the Signal-to-Noise Ratio (SNR) of the image. A second morphological opening step is performed to discard all connected components having less than 2 pixels. The resulting binary mask is demonstrated in Fig. 2g. In the end, the centroids of all remaining connected components in the binary mask are taken as measurements, consisting of the two-dimensional
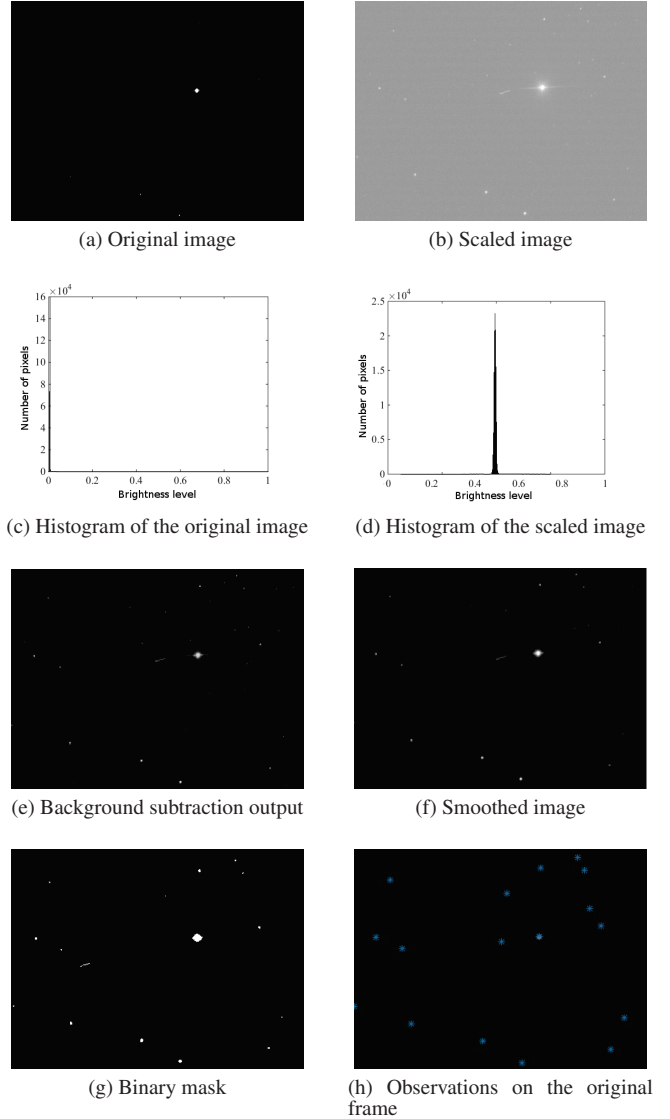


(a) Original image

(b) Scaled image

(c) Histogram of the original image

(d) Histogram of the scaled image

(e) Background subtraction output

(f) Smoothed image

(g) Binary mask

(h) Observations on the original frame

**Figure 2**: **Preprocessing work flow**

positions in the respective image frame. Hence, all results shown in Sec. 7 are measured in pixels.

The final observations in the sample image 2a resulting from the proposed extraction method are demonstrated in Fig. 2h.

# 6. SIMULATION

There is no way of obtaining *a priori* information about the telescope drift, therefore a suitable simulation method is required. However, the nature of the application does not require a completely realistic image simulation, thus a simplistic, yet functional model is considered. For multi-object estimation, it is essential to have a realistic pattern of stars in the background, and moving targets in the sensor FoV. Furthermore, two modes of sensor drift have to be simulated: random jitter of the sensor in the horizontal coordinate system is modelled as Brownian motion, and possible uncompensated diurnal motion is approximated by a Near Constant Velocity (NCV) motion of the celestial sphere with
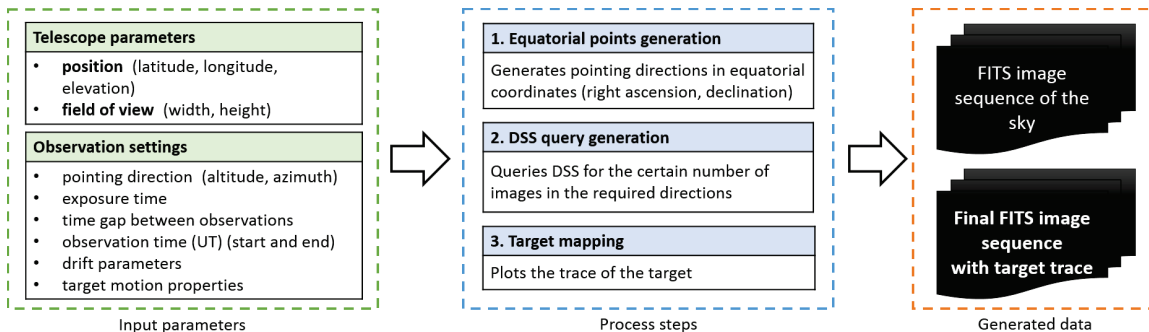
**Figure 3**: **Simulation work flow (DSS: Digital Sky Survey)**

respect to the sensor due to the Earth motion.

The overview of the simulation work-flow is shown in Fig. 3. The main process consists of three main steps: generation of the telescope orientation in equatorial coordinates, sky background extraction and target mapping.

The first step is essentially a geometrical conversion of a simulated telescope pointing direction to the position in the sky given in equatorial coordinates. As the time passes, celestial objects shift with respect to the observer due to diurnal motion. In this way, a slightly different area in the sky is captured for every time step, creating the effect of a linear drift compromised by a small acceleration noise (Eq. (12)). The Brownian drift of the sensor is generated in horizontal coordinates as a small pointing direction error of the telescope. In this step, the time and duration of the observation, the position of the telescope and its pointing direction are used to generate a sequence of equatorial coordinates.

As a second step, the star background is generated. The list of equatorial coordinates, together with the FoV of the telescope, are used for the extraction of the corresponding patch of the sky from the Digital Sky Survey (DSS) provided by European Southern Observatory on-line archive [21].[4] Since these images have an extremely high SNR (see Fig. 4a) which is likely to be much lower in reality due to low exposure times used for debris tracking, only the brightest stars that can outshine the photon noise of the background are used for further processing.

Then, the target is projected on the star pattern. Its position in every frame of the image sequence is determined by two initial values: the starting position of the satellite on the sky and its angular velocity. The length of the target track depends on the parameters of the shutter speed and the velocity of the target. A resulting image is shown in Fig. 4b.

As it was mentioned above, the Brownian drift is generated in horizontal coordinates (azimuth and altitude of the telescope pointing direction) and thus is measured in degrees. On the other hand, the proposed method corrects for the values in the image space, given in pixels. To be able to compare ground truth values with the drift recovered, the original variation in horizontal coordinates is therefore mapped from degrees to pixels. An example of a purely Brownian drift and of a composite drift mixing a Brownian and a NCV component, are shown in Fig. 5.

---

[4]The extracted data is copyrighted by the Space Telescope Science Institute (STScI Digitized Sky Survey, 1993, 1994, AURA, Inc. all rights reserved).
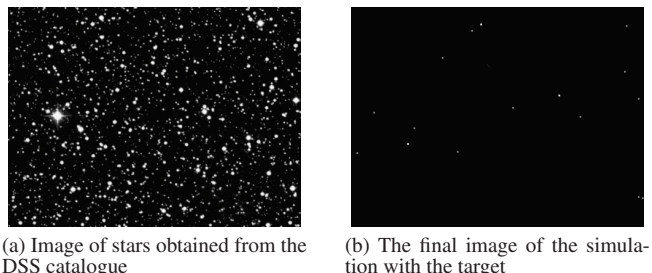


(a) Image of stars obtained from the DSS catalogue

(b) The final image of the simulation with the target

**Figure 4**: **Simulation steps**

## 7. RESULTS

The section presents the results of experiments on the proposed drift compensation model, exploiting both simulated data and real data, and analyses its performances.

*Sensor observation model*

The single-object/single-observation likelihood function $g_t$ depends on the sensor state $y_t$ as follows:

$$g_t(z|x_t, y_t) = \mathcal{N}(z; H(x_t - y_t), Q_{m,t}), \qquad (7)$$

where $\mathcal{N}(\cdot; \mu, \sigma)$ denotes a Gaussian distribution with mean $\mu$ and covariance $\sigma$, $H$ is the observation matrix given by

$$H = \begin{bmatrix} \mathbf{I}_2 & \mathbf{0}_2 \end{bmatrix}, \qquad (8)$$

and $Q_{m,t}$ is a noise covariance matrix of the form

$$Q_{m,t} = (\sigma_{m,t})^2 \mathbf{I}_2, \qquad (9)$$

where the standard deviation $\sigma_{m,t}$ is a model parameter. On the other hand, the probability of detection $p_{d,t}$ and the clutter intensity $\lambda_t c_t$ are assumed independent from the sensor state $y_t$. In addition, the spatial distribution of the clutter is $c_t$ is modelled as a uniform distribution on the sensor FoV.

*Sensor motion models*

Two different sensor motion models (2) were considered, accounting for drifts of specific nature arising from two different modes of telescope operation.

*Brownian model*—The Brownian model describes an operation mode where the diurnal motion of the earth is corrected by the telescope, but the observation is corrupted by sensor
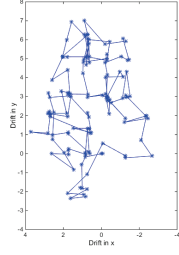
(a) Brownian drift
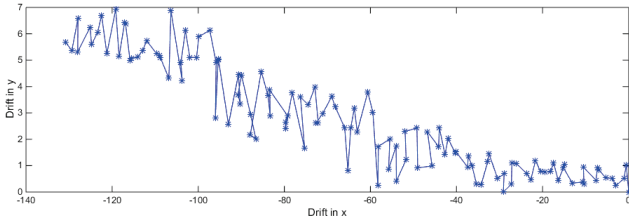


(b) Composite drift

**Figure 5**: **Examples of simulated sensor drift, in the image frame, over 120 time steps. Note the scale difference in $x$ and $y$ in Fig. 5b.**

jitter. The Brownian sensor drift $h^{\mathrm{b}}_{t|t-1}$ is modelled as follows:

$$h^{\mathrm{b}}_{t|t-1}(y_t|y_{t-1}) = \mathcal{N}(y_t; y_{t-1}, Q_{\mathrm{b},t}), \qquad (10)$$

where $Q_{\mathrm{b},t}$ is a covariance matrix of the form

$$Q_{\mathrm{b},t} = (\sigma_{\mathrm{b},t})^2 \begin{bmatrix} \Delta_t \mathbf{I}_2 & \mathbf{0}_2 \\ \mathbf{0}_2 & \mathbf{0}_2 \end{bmatrix} \qquad (11)$$

with $\Delta_t$ being the duration since the previous time step in unit time, and the standard deviation $\sigma_{\mathrm{b},t}$ being a model parameter.

*Composite model*—The composite motion describes a static mode of the telescope in which the uncompensated diurnal motion of the earth induces a linear drift, through a NCV model [22], also corrupted by additional sensor jitter, through a Brownian model. The composite sensor drift $h^{\mathrm{c}}_{t|t-1}$ can thus be described as follows. First, an intermediate state $\tilde{y}_t$ is sampled following a NCV model, i.e.

$$\tilde{y}_t \sim \mathcal{N}(\cdot; A_{\ell,t} y_{t-1}, Q_{\ell,t}), \qquad (12)$$

where $A_{\ell,t}$ is the transition matrix given by

$$A_{\ell,t} = \begin{bmatrix} \mathbf{I}_2 & \Delta_t \mathbf{I}_2 \\ \mathbf{0}_2 & \mathbf{I}_2 \end{bmatrix}, \qquad (13)$$

and $Q_{\ell,t}$ is a covariance matrix of the form

$$Q_{\ell,t} = (\sigma_{\ell,t})^2 \begin{bmatrix} \frac{\Delta_t^3}{3}\mathbf{I}_2 & \frac{\Delta_t^2}{2}\mathbf{I}_2 \\ \frac{\Delta_t^2}{2}\mathbf{I}_2 & \Delta_t \mathbf{I}_2 \end{bmatrix}, \qquad (14)$$

the standard deviation $\sigma_{\ell,t}$ being a model parameter. Then, the intermediate state is augmented with a Brownian noise as showm in Eq. (10), i.e.

$$y_t \sim \mathcal{N}(\cdot; \tilde{y}_t, Q_{\mathrm{b},t}). \qquad (15)$$

An example of composite drift simulated over a scenario of 120 time steps in depicted in Fig. 5.

*Object motion models*

We consider two different object motion models.

The first model $f_t^{(1)}$ accounts for near-static objects in the image background. It is modelled as follows:

$$f_t^{(1)}(x_t|x_{t-1}) = \mathcal{N}(x_t; x_{t-1}, Q_{\mathrm{p},t}^{(1)}), \qquad (16)$$

where $Q_{\mathrm{p},t}^{(1)}$ is a covariance matrix of the form

$$Q_{\mathrm{p},t}^{(1)} = (\sigma_{\mathrm{p},t}^{(1)})^2 \begin{bmatrix} \Delta_t \mathbf{I}_2 & \mathbf{0}_2 \\ \mathbf{0}_2 & \mathbf{0}_2 \end{bmatrix}, \qquad (17)$$

where the standard deviation $\sigma_{\mathrm{p},t}^{(1)}$ is a parameter of the model, set to a small value.

The second model $f_t^{(2)}$ accounts for objects passing the sensor FoV. It is designed with a NCV model similarly to Eqs. (13), (14), that is:

$$f_t^{(2)}(x_t|x_{t-1}) = \mathcal{N}(x_t; A_{\ell,t} x_{t-1}, Q_{\mathrm{p},t}^{(2)}), \qquad (18)$$

where $Q_{\mathrm{p},t}^{(2)}$ is a covariance matrix of the form

$$Q_{\mathrm{p},t}^{(2)} = (\sigma_{\mathrm{p},t}^{(2)})^2 \begin{bmatrix} \frac{\Delta_t^3}{3}\mathbf{I}_2 & \frac{\Delta_t^2}{2}\mathbf{I}_2 \\ \frac{\Delta_t^2}{2}\mathbf{I}_2 & \Delta_t \mathbf{I}_2 \end{bmatrix}, \qquad (19)$$

where the standard deviation $\sigma_{\mathrm{p},t}^{(2)}$ is a parameter of the model.

*Input data*

Two real datasets were collected for these experiments, during the close passage of asteroid 2007HA on Apr 17, 2007. The first one was collected at 20:50:26 UT, over $19\,\mathrm{min}$ and has 38 frames, the second one at 21:53:53 UT, over $15\,\mathrm{min}$ and has 26 frames.

In addition, two simulated datasets were generated following the procedure explained in Sec. 6. The first dataset was corrupted with a Brownian drift and the second one with a composite drift. The variance of the Brownian pointing direction error was set to $4.32 \times 10^{-4\prime\prime}$. As for the other parameters of the simulation, they were set to realistic empirical values as follows: the exposure time of the sensor was set to $2\,\mathrm{s}$ and CCD reading time to $0.5\,\mathrm{s}$. The telescope would be located at $70°24'15''$ N, $24°37'38''$ W. The hypothetical observation was made on Aug 23, 2013 at 22:10 and lasted for $5\,\mathrm{min}$. The velocity of the satellites was set to an angular rate of $7.26 \times 10^{-5}\,\mathrm{rad\,s^{-1}}$.

*Parametrisation*

The implementation of the PHD filters follow a Gaussian Mixture (GM) approach as described in [23]. In addition, we follow a measurement-driven approach [24], [25] in order to avoid the initialisation of many superfluous birth components.

The parametrisation of the filters for the experiments is given in Table 1. Note that the probability of detection $p_{\mathrm{d},t}$ is set to different values for the real and simulated data and reflects the quality of the observation process in both cases.

*Results on simulated data*

The first simulated scenario involves an observation process over 120 time steps corrupted by a Brownian sensor drift,

6

**Table 1**: **Parametrisation**

| 1. Multi-object filter (time $t$) | | | |
|---|---|---|---|
| Parameter | | Sim. data | Real data |
| Prob. of survival (static) | $p_{\mathrm{s},t}^{(1)}$ | 0.98 | 0.9 |
| Prob. of survival (NCV) | $p_{\mathrm{s},t}^{(2)}$ | 0.98 | 0.9 |
| Std. dev. (static) | $\sigma_{\mathrm{p},t}^{(1)}$ | $10^{-3}$ | $10^{-3}$ |
| Std. dev. (NCV) | $\sigma_{\mathrm{p},t}^{(2)}$ | 1 | 1 |
| Prob. of detection | $p_{\mathrm{d},t}$ | 0.9 | 0.6 |
| Std. dev. (obs.) | $\sigma_{\mathrm{m},t}$ | $10^{-3}$ | $10^{-3}$ |
| Clutter rate | $\lambda_t$ | 0.1 | 0.2 |

| 2. Sensor state estimator (time $t$) | | | |
|---|---|---|---|
| Parameter | | Sim. data | Real data |
| Particle number | $N$ | 100 | 400 |
| Std. dev. (Brownian) | $\sigma_{\mathrm{b},t}$ | 1 | 1 |
| Std. dev. (linear) | $\sigma_{\ell,t}$ | 1 | 1 |
| Resampling threshold | $\tau$ | 0.1 | 0.1 |

simulated as described in Sec. 6. The sensor estimator is accordingly fed with a Brownian drift model using the parametrisation as given in Table 1.

Fig. 6 depicts the observations and filter outputs of the first scenario. The filter output shows that the spread of each estimated star position is very limited and the trajectory of the moving object closely approximates a straight line. This suggests that the sensor drift was accurately compensated by the filter; Fig. 7 indeed shows that the estimation error in the drift remained below 0.2 pixels on each axis throughout the scenario.
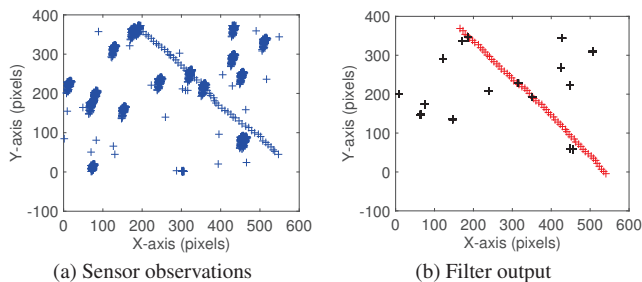


(a) Sensor observations     (b) Filter output

**Figure 6**: **Simulated scenario with Brownian drift. Observations (resp. stars, moving objects) are depicted with blue (resp. black, red) crosses.**

The second simulated scenario involves an observation process over 120 time steps, corrupted by a composite sensor drift as detailed in Sec. 6. The sensor estimator now works with a composite drift model using the parameters as given in Table 1.

Fig. 8 depicts the observations and filter outputs of the second scenario. Similarly to the first scenario, the filter proves to be effective in the classification of objects between moving targets and stars and also in the estimation of the object states. Again, the quality of the multi-object estimation is backed by an accurate estimation of the sensor drift as demonstrated in Fig. 9.
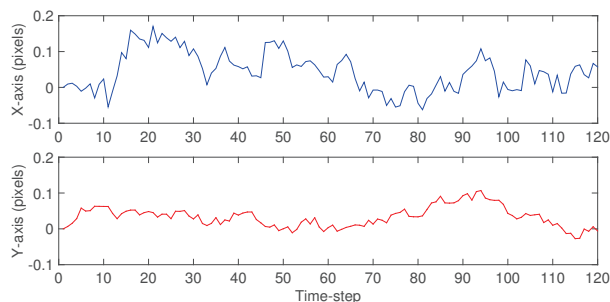


**Figure 7**: **Error in the drift estimation on the simulated scenario with Brownian drift.**
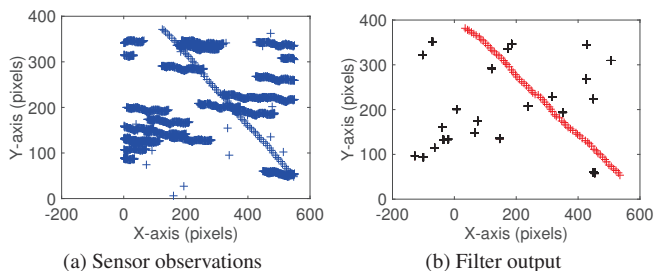


(a) Sensor observations     (b) Filter output

**Figure 8**: **Simulated scenario with composite drift. Observations (resp. stars, moving objects) are depicted with blue (resp. black, red) crosses.**

*Results on real data*

For the first dataset, the sensor estimator assumes a Brownian drift model and for the second one, it assumes a composite drift model. The parametrisation is given in Table 1. The output of the two experiments is shown in Fig. 10 and 11.

Overall, the proposed method proved to be successful in classifying the moving objects from the stars and estimating the positions of the objects in the image sequences provided by both real datasets. An objective assessment of the proposed drift compensation method is lacking in this context since the ground truth associated to the real datasets is unknown, but the comparison of the cumulated observations and the estimated positions of the stars suggests that the sensor drift is accurately compensated in both datasets since the stars are registered with a very small internal variation. A comparison of this approach with an image-based registration method in a biomedical context can be found in [26].

Note that while a continuous trajectory for the passage of asteroid 2007H in the first dataset can be extracted from the estimated positions of the moving object in the successive frames (red crosses in Fig. 10), the asteroid in the second dataset is initially misclassified as a static object due to the close proximity of a bright star in that region which is causing missed detections of nearby objects (see Fig. 11).

## 8. CONCLUSIONS

A new method was proposed to simultaneously estimate the motion of the sensor and the trajectories of targets with different motion models in astronomical images. For this purpose, a hierarchical process was used which incorporates a PHD filter with classification. No prior information about
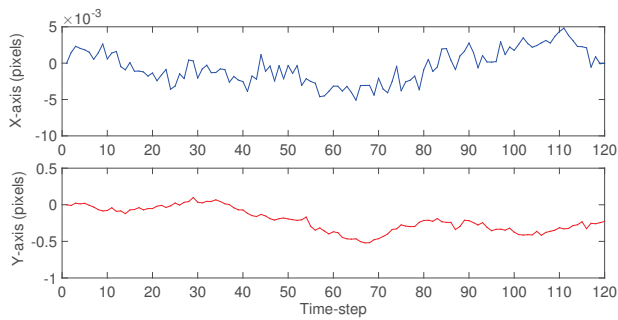
**Figure 9**: Error in the drift estimation on the simulated scenario with composite drift.



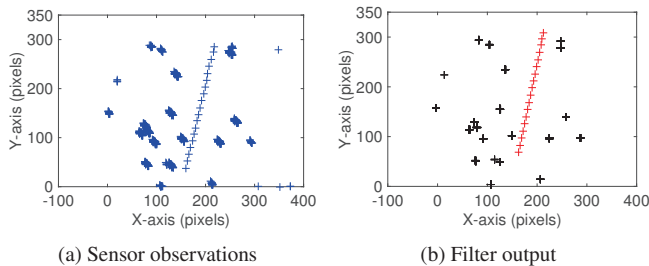(a) Sensor observations     (b) Filter output

**Figure 10**: First real dataset (close passage of asteroid 2007HA), processed with a Brownian sensor drift. Observations (resp. stars, moving objects) are depicted with blue (resp. black, red) crosses. The spacecraft first appeared at the bottom of the camera frame.
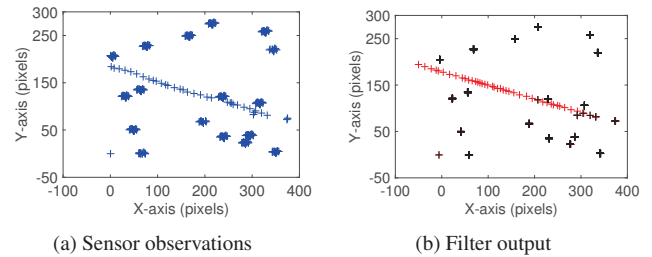


(a) Sensor observations     (b) Filter output

**Figure 11**: Second real dataset (close passage of asteroid 2007HA), processed with a composite sensor drift. Observations (resp. stars, moving objects) are depicted with blue (resp. black, red) crosses. The spacecraft first appeared on the right-hand side of the camera frame.

the telescope position or its pointing direction is necessary since it is solely based on the images acquired through the telescope.

The method was tested on simulated and real data and performed well on two types of drift that typically occur in astronomical observation. Furthermore, the method not only estimates the sensor drift but also provides information on the object type through its specific motion behaviour in the field of view. Due to the hierarchical structure of the algorithm, the bias estimation inherits its robustness to imperfections in the data from the underlying PHD filter framework.

For the validation of the presented framework, a simple observation extraction scheme was proposed. A method for the simulation of astronomical images with a moving target was developed; it is capable of generating an image of the sky from any geographical position at any given date or time with an orbital object track plotted with specific parameters. The resulting data sets were suitable for the given task and might also be useful for similar applications.

## ACKNOWLEDGMENTS

## REFERENCES

[1] D. Mehrholz, L. Leushacke, W. Flury, R. Jehn, H. Klinkrad, and M. Landgraf, "Detecting, tracking and imaging space debris," *ESA Bulletin(0376-4265)*, no. 109, pp. 128–134, 2002.

[2] U.S. Strategic Command website, www.stratocom.mil, January 2014.

[3] European Space Agency website, www.esa.int, April 2013.

[4] J. Cheng, *The principles of astronomical telescope design*. Springer, 2009.

[5] P. Bely, *The design and construction of large optical telescopes*. Springer Science & Business Media, 2003.

[6] P. T. Wallace, "A rigorous algorithm for telescope pointing," in *Astronomical Telescopes and Instrumentation*. International Society for Optics and Photonics, 2002, pp. 125–136.

[7] M. Trueblood and R. M. Genet, "Telescope control," 1997.

[8] M. Warner, V. Krabbendam, and G. Schumacher, "Adaptive periodic error correction for heidenhain tape encoders," in *SPIE Astronomical Telescopes+ Instrumentation*. International Society for Optics and Photonics, 2008, pp. 70 123N–70 123N.

[9] F. J. Masci, D. Makovoz, and M. Moshir, "A robust algorithm for the pointing refinement and registration of astronomical images," *Publications of the Astronomical Society of the Pacific*, vol. 116, no. 823, pp. 842–858, 2004.

[10] B. Zitova and J. Flusser, "Image registration methods: a survey," *Image and vision computing*, vol. 21, no. 11, pp. 977–1000, 2003.

[11] R. W. H. van Bezooijen, L. Degen, and H. Nichandros, "Guide star catalog for the Spitzer space telescope pointing calibration and reference sensor," in *Astronomical Telescopes and Instrumentation*. International Society for Optics and Photonics, 2004, pp. 253–265.

[12] Y. A. Azzam, K. Kosuge, Z. Wang, A. A. Alawy, and Y. Hirata, "Telescope Automatic Alignment and Pointing using Pattern Matching," in *The 4h International Conference of Advanced Mechatronics (ICAM04), Asahikawa, Hokaido, Japan, 3-5 Oct*, 2004.

[13] A. Swain and D. Clark, "The single-group PHD filter: an analytic solution," in *Information Fusion (FUSION),*

*2011 Proceedings of the 14th International Conference on*.   IEEE, 2011, pp. 1–8.

[14] C. S. Lee, D. E. Clark, and J. Salvi, "SLAM with dynamic targets via single-cluster PHD filtering," *Selected Topics in Signal Processing, IEEE Journal of*, vol. 7, no. 3, pp. 543–552, 2013.

[15] B. Ristic, D. E. Clark, and N. Gordon, "Calibration of multi-target tracking algorithms using non-cooperative targets," *Selected Topics in Signal Processing, IEEE Journal of*, vol. 7, no. 3, pp. 390–398, 2013.

[16] J. Houssineau, D. Clark, S. Ivekovic, C. S. Lee, and J. Franco, "A unified approach for multi-object triangulation, tracking and camera calibration," *arXiv preprint arXiv:1410.2535*, 2014.

[17] I. Schlangen, J. Houssineau, and D. Clark, "A novel approach to image calibration in super-resolution microscopy," in *Control, Automation and Information Sciences (ICCAIS), 2014 International Conference on*. IEEE, 2014, pp. 111–116.

[18] R. P. S. Mahler, "Multitarget Bayes filtering via first-order multitarget moments," *Aerospace and Electronic Systems, IEEE Transactions on*, vol. 39, no. 4, pp. 1152–1178, 2003.

[19] J. Houssineau, D. E. Clark, and P. Del Moral, "A sequential Monte Carlo approximation of the HISP filter," in *European Signal Processing Conference (EU-SIPCO)*, 2015.

[20] N. J. Gordon, D. J. Salmond, and A. F. M. Smith, "Novel approach to nonlinear/non-Gaussian Bayesian state estimation," in *IEE Proceedings F (Radar and Signal Processing)*, vol. 140, no. 2.   IET, 1993, pp. 107–113.

[21] European Southern Observatory website, www.eso.org, March 2015.

[22] X. R. Li and V. P. Jilkov, "Survey of maneuvering target tracking. Part I. Dynamic models," *Aerospace and Electronic Systems, IEEE Transactions on*, vol. 39, no. 4, pp. 1333–1364, 2003.

[23] B.-N. Vo and W.-K. Ma, "The Gaussian mixture probability hypothesis density filter," *Signal Processing, IEEE Transactions on*, vol. 54, no. 11, pp. 4091–4104, 2006.

[24] J. Houssineau and D. Laneuville, "PHD filter with diffuse spatial prior on the birth process with applications to GM-PHD filter," in *Information Fusion (FUSION), 2010 13th Conference on*.   IEEE, 2010, pp. 1–8.

[25] B. Ristic, D. Clark, and B.-N. Vo, "Improved SMC implementation of the PHD filter," in *Information Fusion (FUSION), 2010 13th Conference on*.   IEEE, 2010, pp. 1–8.

[26] I. Schlangen, J. Franco, J. Houssineau, W. T. E. Pitkeathly, D. Clark, I. Smal, and C. Rickman, "Markerless stage drift correction in super-resolution microscopy using the single-cluster PHD filter," *Accepted to: IEEE Journal on Selected Topics in Signal Processing (JSTSP), Special Issue on Advanced Signal Processing in Microscopy and Cell Imaging*, 2016.

## BIOGRAPHY

***Oksana Hagen*** *received a joint M.Sc. degree in Vision and Robotics from the Universities of Burgundy (France), Girona (Spain), and Heriot-Watt University (Edinburgh, UK) in 2015 with distinction.   Her thesis was focused on multi-object estimation in space-situational awareness context.  She was awarded a B.Sc. degree in Electrical and Computer Engineering from National Chiao Tung University (Taiwan) in 2013.*

***Jérémie Houssineau*** *received an Eng. degree in mathematical and mechanical modelling from MATMECA, Bordeaux, and a M.Sc. degree in mathematical modelling and statistics from the University of Bordeaux, both in 2009.  From 2009 to 2011, he was a Research Engineer with DCNS, Toulon, and then with INRIA Bordeaux. He received his Ph.D. degree in statistical signal processing from Heriot-Watt University, Edinburgh, in 2015.  His research interests include applied probability, point process theory and multi-object estimation.*

***Isabel Schlangen*** *is a current Ph.D. studentship holder at the Edinburgh Super-Resolution Imaging Consortium, UK. She received a German diploma in Mathematics from the University of Bonn (Germany) in 2012 and a joint MSc degree in Vision and Robotics from the Universities of Burgundy (France), Girona (Spain), and Heriot-Watt (Edinburgh, UK) in 2014.  Her current research interests are multi-target estimation, probability theory and image analysis in a mainly biomedical context.*

***Emmanuel D. Delande*** *received an Eng. degree from the Ecole Centrale de Lille, Lille, and a M.Sc. degree in automatic control and signal processing from the University of Science & Technology, Lille, both in 2008. He was awarded his Ph.D. in 2012 from the Ecole Centrale de Lille.   He is a research associate at Heriot-Watt University in Edinburgh. His research interests are in the design and the implementation of multi-object filtering solutions for multiple target tracking and sensor management problems.*

**Jose Franco** received a B.Sc. degree in mathematical engineering from EAFIT University in 2010 and a M.Sc. in computer vision and robotics jointly from the University of Burgundy, the University of Girona and Heriot-Watt University in 2013. He is currently a doctoral student in Heriot Watt University under the supervision of Dr Daniel Clark, where he studies multiple object estimation techniques for a variety of applications.

**Daniel E. Clark** is an Associate Professor in the School of Engineering and Physical Sciences at Heriot-Watt University. His research interests are in the development of the theory and applications of multi-object estimation algorithms for sensor fusion problems. He has led a range of projects spanning theoretical algorithm development to practical deployment. He was awarded his Ph.D. in 2006 from Heriot-Watt University.